Air–Sea Fluxes over the Gulf Stream Region: Atmospheric Controls and Trends

JEFFREY SHAMAN, R. M. SAMELSON, AND ERIC SKYLLINGSTAD

College of Oceanic and Atmospheric Sciences, Oregon State University, Corvallis, Oregon

(Manuscript received 29 May 2009, in final form 11 January 2010)

ABSTRACT

The intraseasonal variability of turbulent surface heat fluxes over the Gulf Stream extension and subtropical mode water regions of the North Atlantic, and long-term trends in these fluxes, are explored using NCEP–NCAR reanalysis. Wintertime sensible and latent heat fluxes from these surface waters are characterized by episodic high flux events due to cold air outbreaks from North America. Up to 60% of the November–March (NDJFM) total sensible heat flux and 45% of latent heat flux occurs on these high flux days. On average 41% (34%) of the total NDJFM sensible (latent) heat flux takes place during just 17% (20%) of the days. Over the last 60 years, seasonal NDJFM sensible and latent heat fluxes over the Climate Variability and Predictability (CLIVAR) Mode Water Dynamic Experiment (CLIMODE) region have increased owing to an increased number of high flux event days. The increased storm frequency has altered average wintertime temperature conditions in the region, producing colder surface air conditions over the North American eastern seaboard and Labrador Sea and warmer temperatures over the Sargasso Sea. These temperature changes have increased low-level vertical wind shear and baroclinicity along the North Atlantic storm track over the last 60 years and may further favor the trend of increasing storm frequency over the Gulf Stream extension and adjacent region.

1. Introduction

The largest wintertime heat fluxes from the ocean to the atmosphere in the North Atlantic occur in the region of the Gulf Stream extension and the adjacent waters of the northwestern portion of the subtropical gyre (Esbensen and Kushnir 1981; Josey et al. 1999). These heat fluxes are supported in the ocean by advective heat convergence in the Gulf Stream and by seasonal heat storage in the surrounding waters, especially the subtropical mode water to the south and east of the Gulf Stream. The subtropical mode water (STMW), or 18°C water, which dominates the upper water column in the northwestern Sargasso Sea, is defined by its relatively homogeneous temperature and salinity and may extend to depths of 500 m or more (Worthington 1959; Marshall et al. 2009). Its vertical homogeneity and consequent weak static stability, which arise from large-scale constraints on the gyre circulation (Dewar et al. 2005), allow the deep penetration of convective vertical exchange in response to wintertime surface cooling events, effectively coupling lower-atmosphere thermodynamic processes to an unusually deep column of ocean water.

The STMW column outcrops in boreal winter along the southern edge of the Gulf Stream in response to these cooling events, which remove a seasonal warm water cap. The temperature and salinity characteristics of STMW are set during this winter season when air–sea heat fluxes in the STMW region and the adjacent Gulf Stream are large. The reemergence of mode water along the Gulf Stream outcrop each winter is a potentially important source of seasonal-to-interannual memory within the climate system. Mode waters possessing temperature and salinity characteristics set during one winter may interact with and influence atmospheric conditions during the next, or a later, winter (Alexander and Deser 1995).

The ocean–atmosphere interactions associated with the wintertime mode water outcrop in the North Atlantic have been examined at a range of time scales. Studies include examinations of STMW decadal variability and its relation to the North Atlantic Oscillation (NAO) (Talley 1996; Joyce et al. 2000), the influences of the atmospheric circulation on turbulent heat fluxes at monthly (Cayan 1992) and weekly time scales (Deser

Corresponding author address: Jeffrey Shaman, 104 COAS Administration Building, Oregon State University, Corvallis, OR 97331.
E-mail: jshaman@coas.oregonstate.edu

DOI: 10.1175/2010JCLI3269.1

and Timlin 1997), and more recent investigation of the effect of synoptic-scale variability on these heat fluxes (Zolina and Gulev 2003).

Interannual variations in heat advection by the Gulf Stream, and the large wintertime air–sea fluxes that the heat advection supports, provide a second potentially important regional influence on the midlatitude atmosphere, as well as on the properties of North Atlantic mode water; this is true also of other western boundary currents in other ocean basins (Kelly et al. 2010). Not only does North Atlantic mode water outcrop and form along the southern edge of the Gulf Stream, but the strong SST gradient across the Gulf Stream creates low-level baroclinicity in the troposphere that anchors storm activity along the SST front (Inatsu et al. 2003; Nakamura et al. 2004, 2008; Brayshaw et al. 2008). These wintertime storms along the Gulf Stream bring cold air across the SST front and elevate surface heat fluxes, contributing to mode water formation.

In general, colder average winter air temperatures produce higher wintertime heat fluxes from the ocean to atmosphere that, in part, drive mode water formation; however, previous studies indicate that synoptic variability creates large changes in air–sea heat fluxes over western boundary currents (Alexander and Scott 1997; Zolina and Gulev 2003; Bond and Cronin 2008), including the Gulf Stream. Consequently, wintertime synoptic variability should be associated with extreme heat flux levels. In essence, the high wintertime heat fluxes in the vicinity of the Gulf Stream extension are generated by the interaction of the more temporally uniform yet spatially heterogeneous ocean surface with the more spatially uniform yet temporally variable atmosphere.

One question we seek to determine in this study is the proportion of total seasonal sensible and latent heat fluxes in the Gulf Stream extension and STMW outcrop region that is due to synoptic events, in particular cold air outbreaks. We hypothesize that synoptic storms are responsible for a large fraction of total seasonal heat fluxes in the Gulf Stream region and that these storms produce synoptic-scale variations of surface turbulent fluxes. Similar synoptic-scale air–sea interactions have been demonstrated for the Southern Ocean (Patoux et al. 2009; Yuan et al. 2009). If discrete events are indeed associated with a large share of the seasonal heat flux in the Gulf Stream region, then further understanding of the weather systems associated with these events, their frequency, and any trends in their occurrence is needed.

Here we quantify the synoptic contribution to total November–March (NDJFM) surface sensible and latent heat fluxes in the North Atlantic Gulf Stream extension and STMW outcrop region. We examine the tropospheric structure associated with high daily wintertime heat fluxes in this region. Trends in the 1948–2007 National Centers for Environmental Prediction (NCEP)–National Center for Atmospheric Research (NCAR) reanalysis record are then described. Changes in storm activity and low-level baroclinicity in the region are examined as well.

Section 2 describes the data used for this analysis. Section 3 categorizes the daily reanalysis record based on surface turbulent flux levels and quantifies the fraction of total seasonal air–sea heat exchange over Gulf Stream extension and STMW outcrop region associated with high heat flux days. Section 4 then examines the tropospheric structure and synoptic characteristics associated with these high heat flux days. Trends in the reanalysis record of synoptic activity for the study region are then described in section 5. Discussion is provided in section 6.

2. Data

This study is part of the Climate Variability and Predictability (CLIVAR) Mode Water Dynamic Experiment (CLIMODE) project (Marshall et al. 2009) for studying ocean–atmosphere interaction in the Gulf Stream and North Atlantic STMW region. The associated region of interest (the ''CLIMODE region'') is here defined as 30°–42°N, 70°–50°W. Analyses were performed using 1948–2008 daily and 1949–2008 monthly 2.5° × 2.5°NCEP–NCAR reanalysis data (Kalnay et al. 1996). Measures include surface sensible and latent heat fluxes, surface and tropospheric temperatures, vertical and horizontal velocities, specific humidity, and geopotential.

For additional comparison, we used the Objectively Analyzed Air–Sea Fluxes (OAFlux) project daily estimates of surface sensible and latent heat fluxes (Yu et al. 2008). These data are derived from satellite retrievals, ship reports, and surface meteorology. Daily data at 1° resolution are available from 1985 to 2006. The time series of November–March seasonal averages of the NCEP–NCAR reanalysis and OAFlux estimates of CLIMODE region sensible and latent heat fluxes showed high interannual correlation ($r = 0.99$ and $r = 0.98$, respectively) and moderate bias of the reanalysis (+9% or $+5.4$ W m^{-2} for the sensible heat flux and −3% or -4.7 W m^{-2} for the latent heat flux).

For this study, we use a threshold daily flux rate (e.g., 100 W m^{-2}) to categorize days as high or low flux events over the CLIMODE region. The slight biases between the NCEP–NCAR reanalysis and OAFlux heat flux estimates might corrupt this categorization; however, our results were found to be insensitive to the precise threshold used (e.g., 100 or 125 W m^{-2}, etc.). The NCEP–NCAR

reanalysis fluxes were used for most of the calculations reported below because of the greater length of the available time series. Additional analyses using voluntary observing ship (VOS) data were also made and are discussed in the appendix.

Previous studies have compared NAO variability with SMTW surface transformation (Talley 1996; Joyce et al. 2000) as well as North Atlantic storm activity (Benedict et al. 2004; Jin et al. 2006; Vallis and Gerber 2008; Gerber and Vallis 2009). We therefore also examined whether turbulent surface fluxes and associated synoptic activity indicators over the Gulf Stream extension and STMW outcrop region, which lie at the western edge of the North Atlantic storm track, are correlated with NAO variability at seasonal and longer time scales. A monthly index of the NAO (available online at http://www.cdc.noaa.gov/ClimateIndices/List/), averaged seasonally for November–March 1948–2007, was used for this analysis. The NAO index values are derived using a rotated principal component analysis of 500-hPa geopotential height anomalies.

3. Heat flux events

Statistical properties of the intraseasonal variability of air–sea fluxes in the CLIMODE region from the NCEP–NCAR reanalysis were examined. These properties include (Figs. 1 and 2) the average daily sensible (latent) heat flux for the CLIMODE region, histograms of the number of ''event days'' per NDJFM season, histograms of the fraction of total NDJFM sensible (latent) heat flux each season due to event days, histograms of the duration in days of sensible (latent) heat flux events, and daily sensible (latent) heat fluxes for the CLIMODE region during 2003 and 2004. Here, event days are defined as those during which sensible (latent) heat fluxes exceed 100 (250) W m^{-2} for the CLIMODE region. These thresholds are somewhat arbitrary; however, their magnitude corresponds to the 83rd (80th) percentile of the 60-yr NDJFM reanalysis record. Using the Coupled Ocean–Atmosphere Response Experiment (COARE) 3.0 bulk algorithm (Fairall et al. 2003), 100 W m^{-2} sensible (250 W m^{-2} latent) heat flux is roughly equivalent to a 6 K (4 K) air–sea temperature difference in the presence of a 10 m s^{-1} wind and 77% relative humidity. Results, including those presented in sections 4 and 5, were found to be insensitive to the precise event day threshold used (e.g., 100 or 125 W m^{-2}, etc.). Results were also insensitive to the use of a daily anomaly threshold that accounted for the variation of average daily heat fluxes within the NDJFM season (Figs. 1a and 2a).

The presented distributions have several noteworthy features. The daily averages are remarkably variable from day to day given the 60-yr average. The highest heat fluxes are of course during winter months (Figs. 1a and 2a); in particular, from November through the end of March sensible (latent) heat fluxes are >40 (>150) W m^{-2}. Based on this climatology we adopt the NDJFM season for the remaining analyses. There is considerable year-to-year variability of the number of event days and the fractional amount of total heat flux accounted for by the event days (Figs. 1b,c and 2b,c). On average, 41% (34%) of total NDJFM sensible (latent) heat flux occurs during only 17% (20%) of NDJFM days. The duration of event histograms (Figs. 1d and 2d) and the 2003 and 2004 time series heat flux plots (Figs. 1e and 2e), which are representative of other individual years, show that event days are typically isolated 1–2-day occurrences. In fact, 81% (77%) of the high sensible (latent) heat events last for less than 3 days.

These findings indicate that a large amount of the wintertime surface fluxes of heat and moisture occur during a relatively small number of days. In addition, these high flux days are often 1–2-day events and thus are likely associated with synoptic weather variability.

4. Event day composites

We next use composite analysis to examine the meteorological conditions associated with CLIMODE region event days. Daily NCEP–NCAR reanalysis fields were composited by averaging all 1948–2007 NDJFM days during which sensible heat fluxes did not exceed 100 W m^{-2} (i.e., ''non-event'' days) and subtracting this average from the average for all event days to obtain mean event-day anomaly fields. Changing the classification of an event day from 100 W m^{-2} sensible heat flux to 125 or 150 W m^{-2} produced little change in the composite results. A similar insensitivity is evident when event day classification is based on latent heat flux rates. In addition, we expanded and contracted the CLIMODE domain and translated the domain up to 5° in all directions (north, south, east, and west); in each instance, composite results were found to be insensitive to these changes.

The composite of surface temperature reveals a marked cold anomaly over eastern North America and little temperature anomaly (<1 K) over the ocean, including the Gulf Stream Extension and Sargasso Sea (Fig. 3a). The mean event-day 1000-hPa geopotential anomaly shows a very specific strong circulation pattern (Fig. 3b). A steep west–east geopotential gradient lies centered at 66°W, which is consistent with strong northerly winds. This composite indicates that high heat flux days are associated with a characteristic circulation anomaly. This circulation is consistent with the intense cold air outbreak and explosive cyclogenesis that has been documented

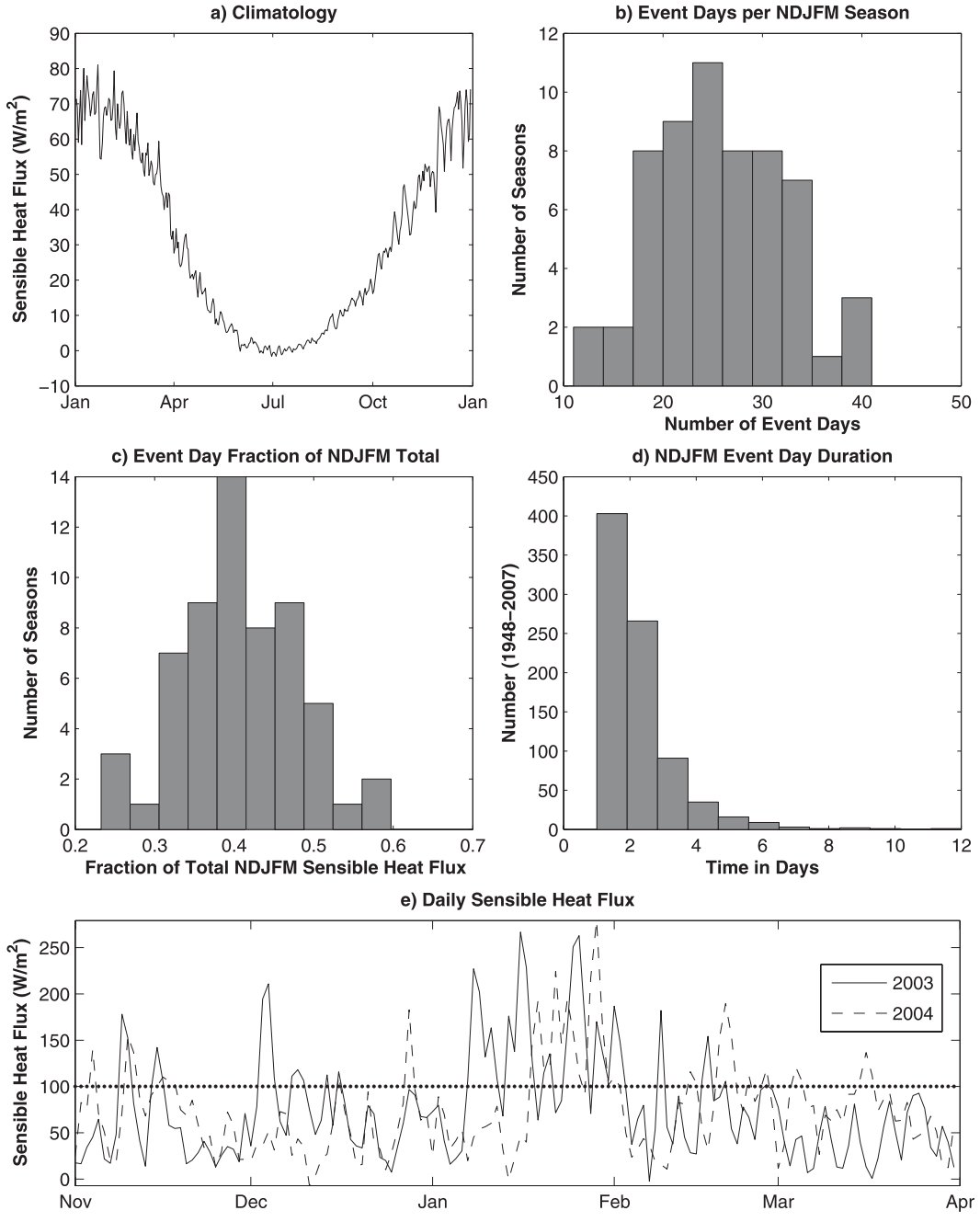

FIG. 1. (a) Plot of average daily 1948–2007 NCEP–NCAR reanalysis sensible heat flux for the CLIMODE region. (b) Histogram of the number of event days per NDJFM season, defined as days during which the average sensible heat flux exceeds 100 W m^{-2}. (c) Histogram of the fraction of total NDJFM sensible heat flux each season occurring during event days. (d) Histogram of the duration in days of each sensible heat flux event for NDJFM 1948–2007. (e) Daily sensible heat fluxes for the CLIMODE region during 2003 and 2004 (year defined by November); the dotted line shows event day threshold 100 W m^{-2}.

over the north and west flanks of the Gulf Stream (Colucci 1976; Sanders and Gyakum 1980; Sanders 1986). Indeed, together the surface temperature and 1000-hPa geopotential composites indicate that high heat flux days are associated with cold air advected off the continent. Average 1000-hPa geopotential fields for event and nonevent days (Figs. 3c,d) show the pronounced circulation change as well, in particular the pronounced ridging and northerly flow that is present along the North American coast during event days (Fig. 3c).

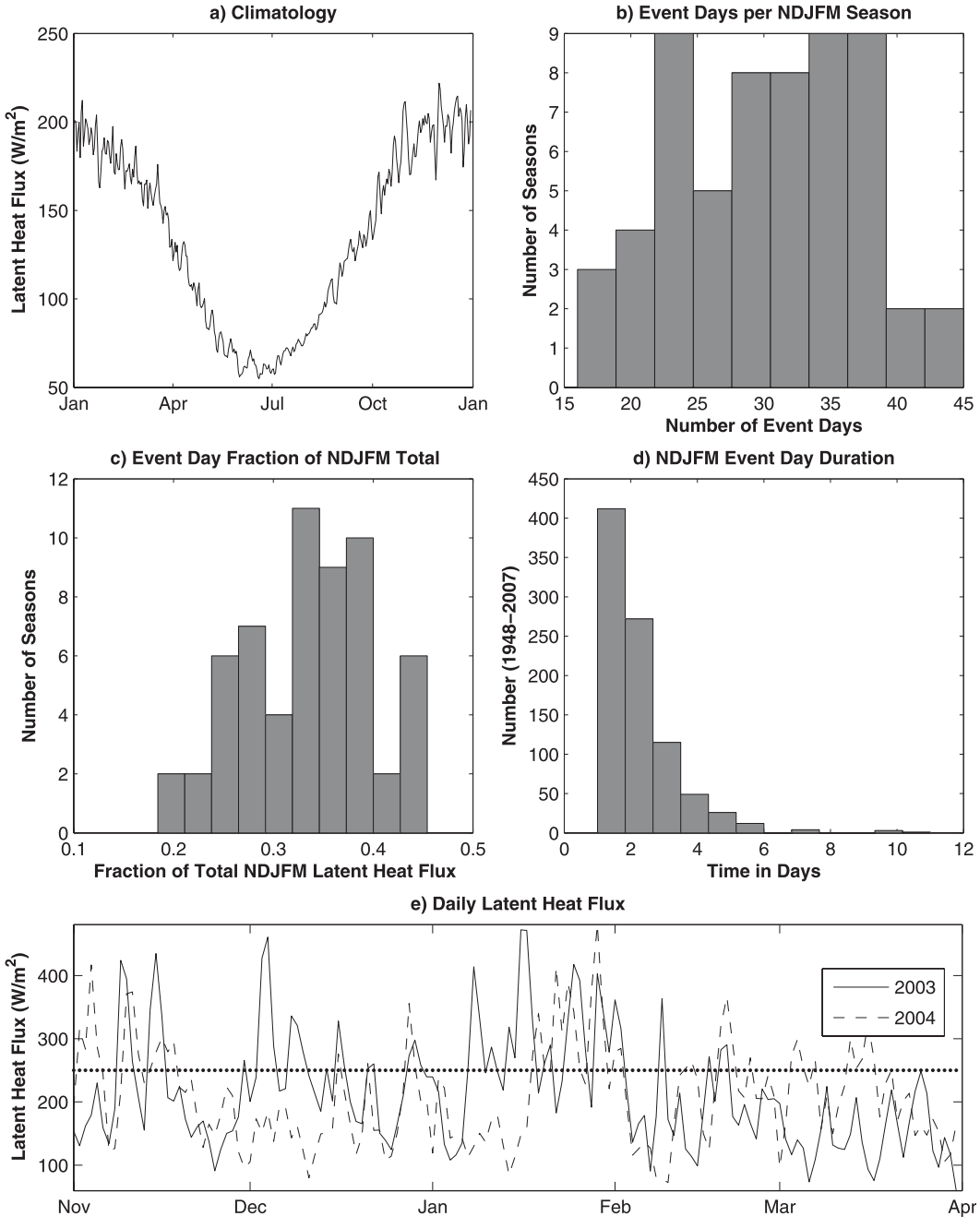

FIG. 2. As in Fig. 1, but for latent heat flux. Here event days are defined as days during which the average latent heat flux exceeds 250 W m^{-2}.

Unlike explicit storm tracking algorithms (e.g., Patoux et al. 2009) or the examination of high-pass-filtered fields (e.g., Alexander and Scott 1997), the composite analysis used here is not a conventional means of identifying storm activity and structure. We did not a priori assume a storm structure but rather used the composite analysis to isolate the anomalous atmospheric conditions over the CLIMODE region when turbulent fluxes are high. The clear cyclone structure and strong geopotential gradient that emerges from this analysis indicates that a characteristic storm structure is typically present during high flux events.

The composite of sensible heat flux, as is to be expected, shows strong positive heat flux anomalies over the CLIMODE region with a maximum at the Gulf Stream extension (Fig. 3e). The 850-hPa wind vector composite

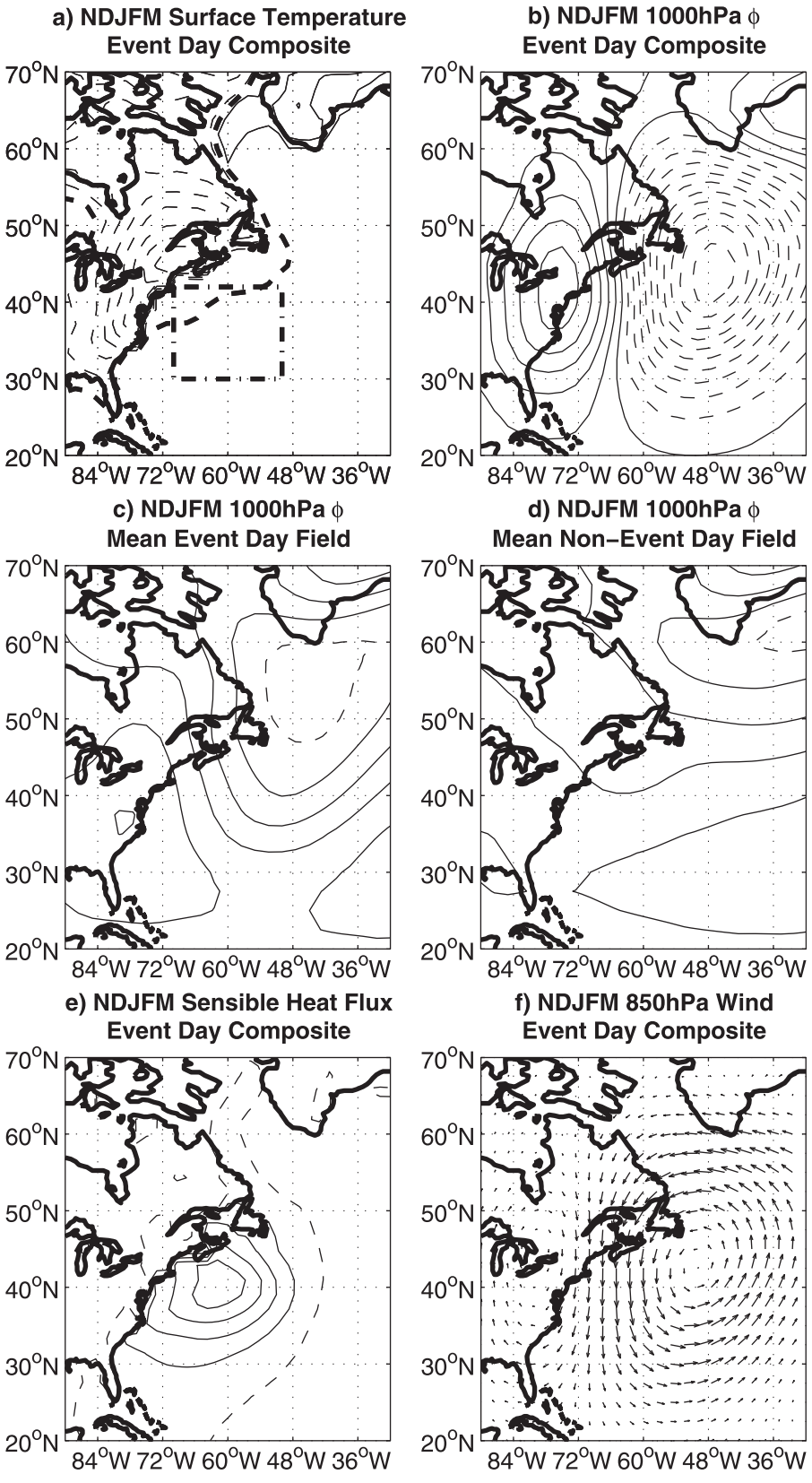
a) NDJFM Surface Temperature
Event Day Composite
b) NDJFM 1000hPa ϕ
Event Day Composite
c) NDJFM 1000hPa ϕ
Mean Event Day Field
d) NDJFM 1000hPa ϕ
Mean Non−Event Day Field
e) NDJFM Sensible Heat Flux
Event Day Composite
f) NDJFM 850hPa Wind
Event Day Composite
70°N
60°N
50°N
40°N
30°N
20°N
84°W 72°W 60°W 48°W 36°W

shows a circulation consistent with the 1000-hPa geopotential composite; in particular, northerly flow between 70° and 60°W and a strong cyclonic circulation centered to the east of the CLIMODE region (Fig. 3f).

These results are consistent with previous findings for the Gulf Stream (Bane and Osgood 1989; Alexander and Scott 1997; Zolina and Gulev 2003) and Kuroshio Extensions (Bond and Cronin 2008), which have shown that synoptic storm activity controls surface turbulent fluxes on synoptic time scales. The combination of the Gulf Stream extension within and jet stream position over the CLIMODE region helps produce the high synoptic variability and these large air–sea flux events (Nakamura et al. 2004). The surface turbulent fluxes destabilize the near-surface troposphere, which increases local baroclinicity, supports storm intensification, and helps maintain the storm track (Hoskins and Valdes 1990; Mak 1998; Inatsu et al. 2003). The storms themselves, that is, the cold air outbreaks, then destroy this baroclinicity through synoptic-scale mixing.

Tropospheric structure and time evolution

The atmospheric circulation anomaly associated with event days extends through the troposphere (Fig. 4). Temperatures warm in the upper troposphere above the near-surface geopotential low. These are indicative of a pronounced dipping of the tropopause and the intrusion of warmer stratospheric air at the 200-hPa level (Hoskins et al. 1985).

Composites of vertically advected specific humidity reveal an anomalous downward flow of dry air over the CLIMODE region in the area of strong anomalous northerly flow (Fig. 4). These anomalies extend throughout the troposphere. To the east is an area of strong moisture ascent, which also extends throughout the troposphere. The northerly flow of these event day storms (~70°W) thus brings cold, dry, descending continental air over the CLIMODE region. This air picks up heat and moisture from the Gulf Stream extension and STMW outcrop, which facilitates mode water formation. Ascending air, along the advancing cold front, carries warmer, moister marine air to the upper troposphere, and possibly lower stratosphere.

Thus, event days produce an exchange of continental and marine air masses, high sensible and latent heat fluxes, and a ventilation of the marine boundary layer. The upper ocean and entire troposphere are coupled. These results are consistent with the model findings of Alexander and Scott (1997) and the observational analysis of Zolina and Gulev (2003). The northerly advection of cold air by synoptic storms across the Gulf Stream front produces the high heat fluxes in the descending cold air wedge that help facilitate mode water formation.

The translation and evolution of event day storm system anomalies can be seen in lagged composites of the reanalysis fields. These lagged composites show the development of anomalies leading up to and following event days. For example, the 2-day prior composite is the average of all days 2 days prior to a NDJFM high flux event day minus the average of all days 2 days prior to a NDJFM nonevent day. Figure 5 shows such lagged composites of the 1000-hPa temperature field from 2 days prior to 2 days after sensible heat flux event days. The eastward and slightly southward translation of storm system temperature anomalies is clearly evident. These temperature anomalies are strongest on the day of and the day prior to the event. Upon crossing the continental margin, Gulf Stream extension, and STMW outcrop, the anomalies weaken rapidly due to strong surface sensible heat fluxes from these ocean waters (Fig. 3e).

5. Linear trends

Over the course of the 60-yr NCEP–NCAR reanalysis record (Fig. 6) and the shorter OAFlux record (Fig. 7), systematic changes in CLIMODE region NDJFM heat fluxes are manifest. There are statistically significant increasing trends of total and event day NDJFM sensible and latent heat fluxes but no significant trend for nonevent day sensible heat fluxes and a statistically

←

FIG. 3. (a) Composites of 1948–2007 NCEP–NCAR reanalysis NDJFM CLIMODE region event days (daily surface sensible heat flux >100 W m^{-2}) minus nonevent days (daily surface sensible heat flux ≤100 W m^{-2}) for the field of surface temperature. Contour intervals are 1 K; negative contours dashed. The −0.5-K contour (dashed and bold) is also shown. The dashed–dotted box delineates the CLIMODE region. (b) As in (a) but for the 1000-hPa geopotential. Contour intervals are 10 m^2 s^{-1}; negative contours dashed. (c) Average 1000-hPa geopotential for all 1948–2007 NDJFM event days. Contour intervals are 40 m^2 s^{-1}; the zero contour is dashed. (d) As in (c) but for nonevent days. (e) As in (a) but for surface sensible heat flux. Contour intervals are 40 W m^{-2}, the zero contour is dashed. (f) As in (a) but for 850-hPa wind.

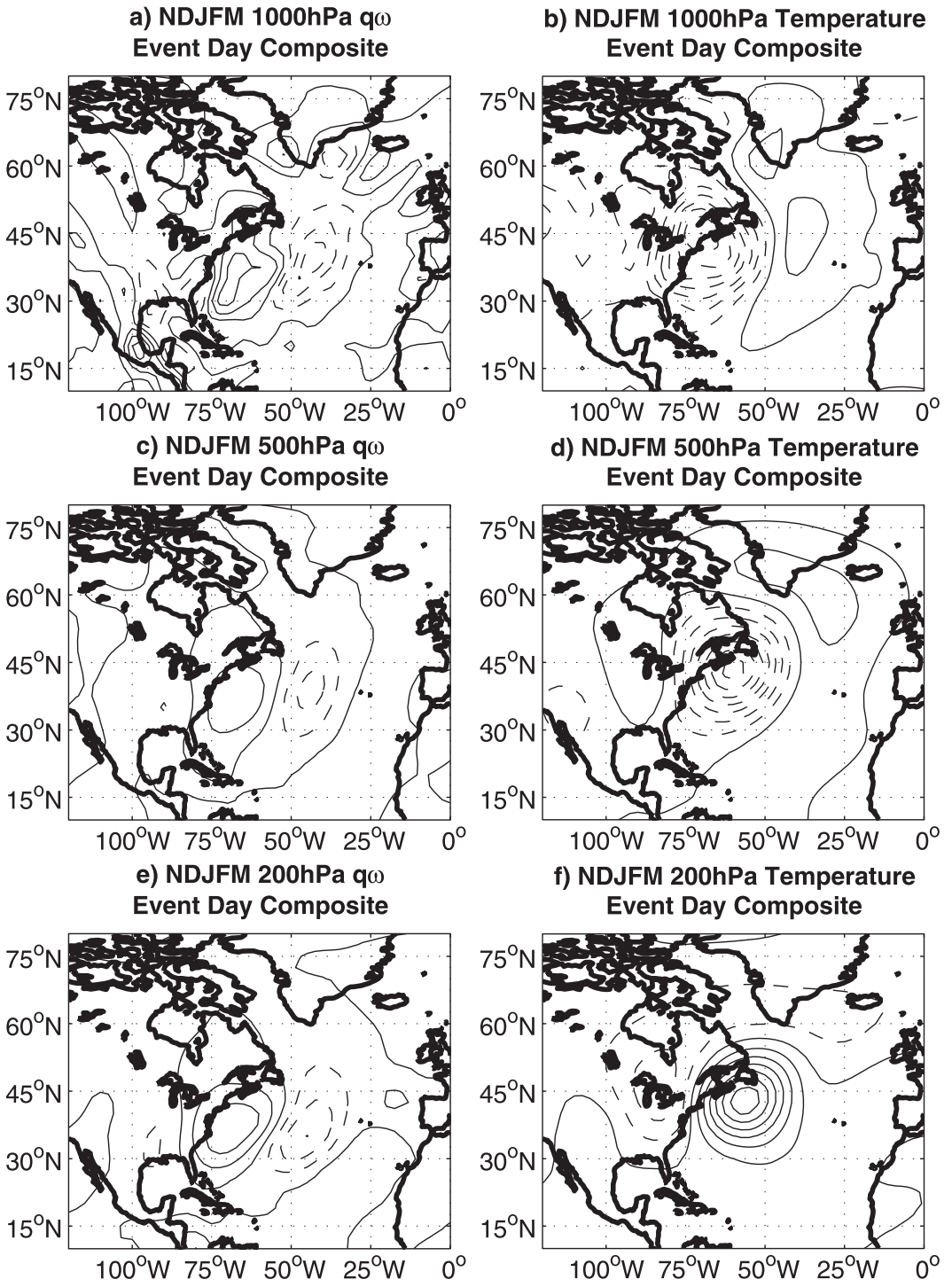

FIG. 4. As in Fig. 3, but for (a),(c),(e) vertically advected moisture and (b),(d),(f) temperature at 1000, 500, and 200 hPa, respectively. Contour intervals are (a),(c) 5×10^{-5} (kg kg^{-1} hPa s^{-1}), (e) 1×10^{-5} (kg kg^{-1} hPa s^{-1}), and (b),(d),(f) 1 K. Negative contours are dashed.

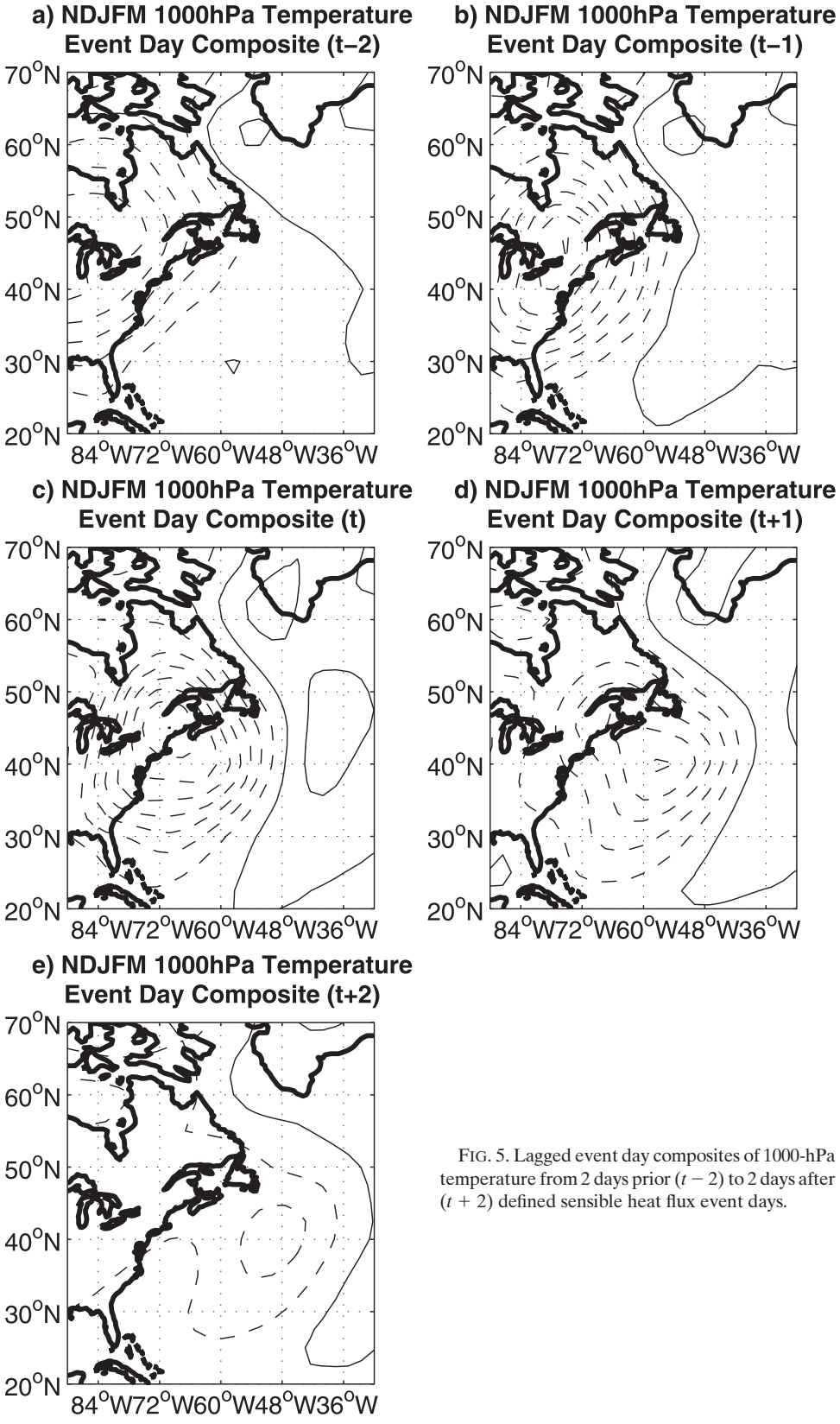

FIG. 5. Lagged event day composites of 1000-hPa temperature from 2 days prior ($t - 2$) to 2 days after ($t + 2$) defined sensible heat flux event days.

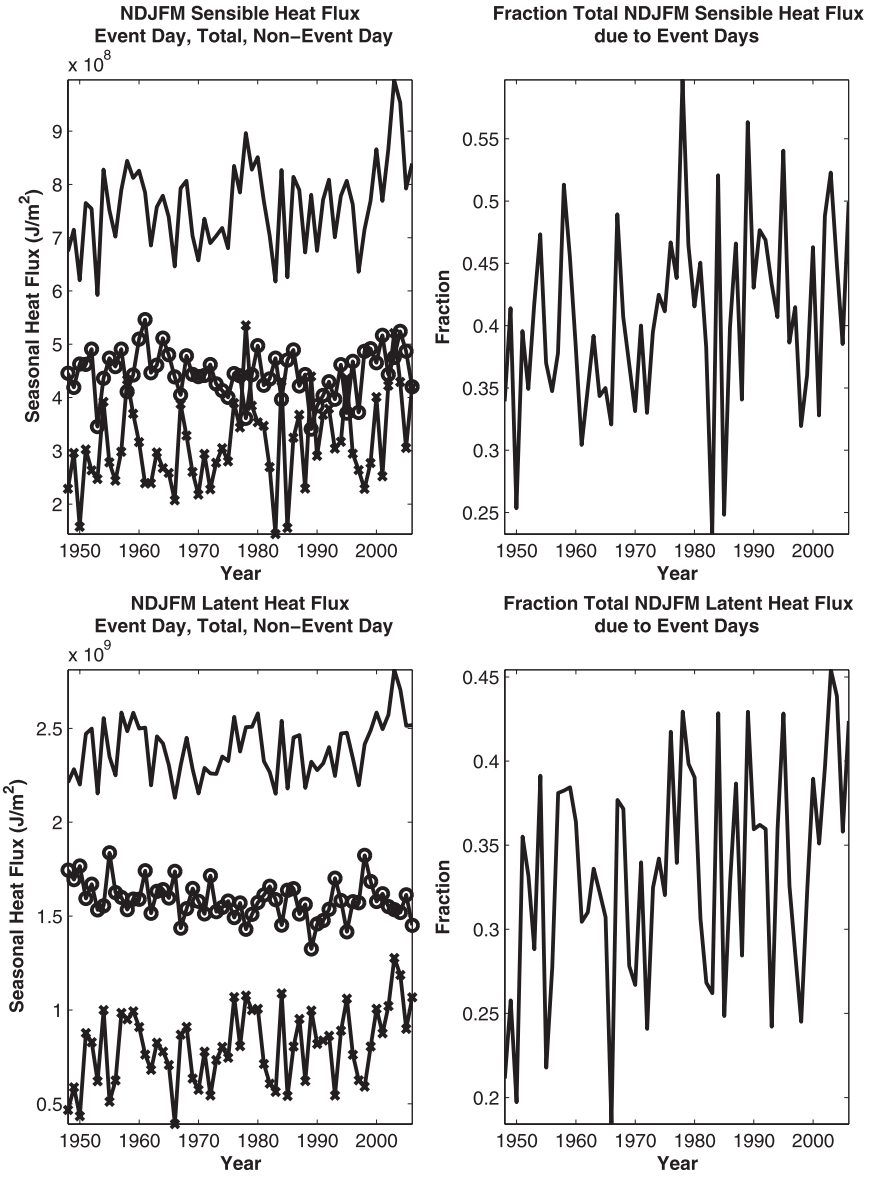

FIG. 6. Time series of 1948–2006 NCEP–NCAR reanalysis NDJFM integrated seasonal heat fluxes. (top left) Time series of seasonal event day (''x'' line), total (event day and nonevent day; solid line), and nonevent day (''o'' line) sensible heat fluxes. (top right) Time series of fraction of the total seasonal sensible heat flux due to event day fluxes. (bottom) As at top, but for latent heat fluxes. Calculations were made using daily reanalysis.

significant decreasing trend for nonevent day latent heat fluxes (Table 1). The fraction of total seasonal heat flux due to event days has also increased with time.

These findings indicate that over the last 60 years the change in surface turbulent fluxes is due to increased synoptic activity, specifically cold air outbreaks, over the CLIMODE region. In addition, the year-to-year variability of the total NDJFM heat flux is most closely linked to event day variability (Figs. 6 and 7). Thus, the NDJFM seasonal heat flux anomalies for the CLIMODE region correspond to anomalies of aggregate seasonal synoptic activity.

Upgrades of the NCEP–NCAR reanalysis model, the introduction and assimilation of satellite observations (Yuan et al. 2009), and changes in the encoding and assimilation of radiosonde data (Harnik and Chang 2003) can all lead to shifts in reanalysis biases that might exaggerate or diminish the apparent linear trends shown here. Many of these changes occurred in the 1970s and some of the flux trends do appear to shift during this

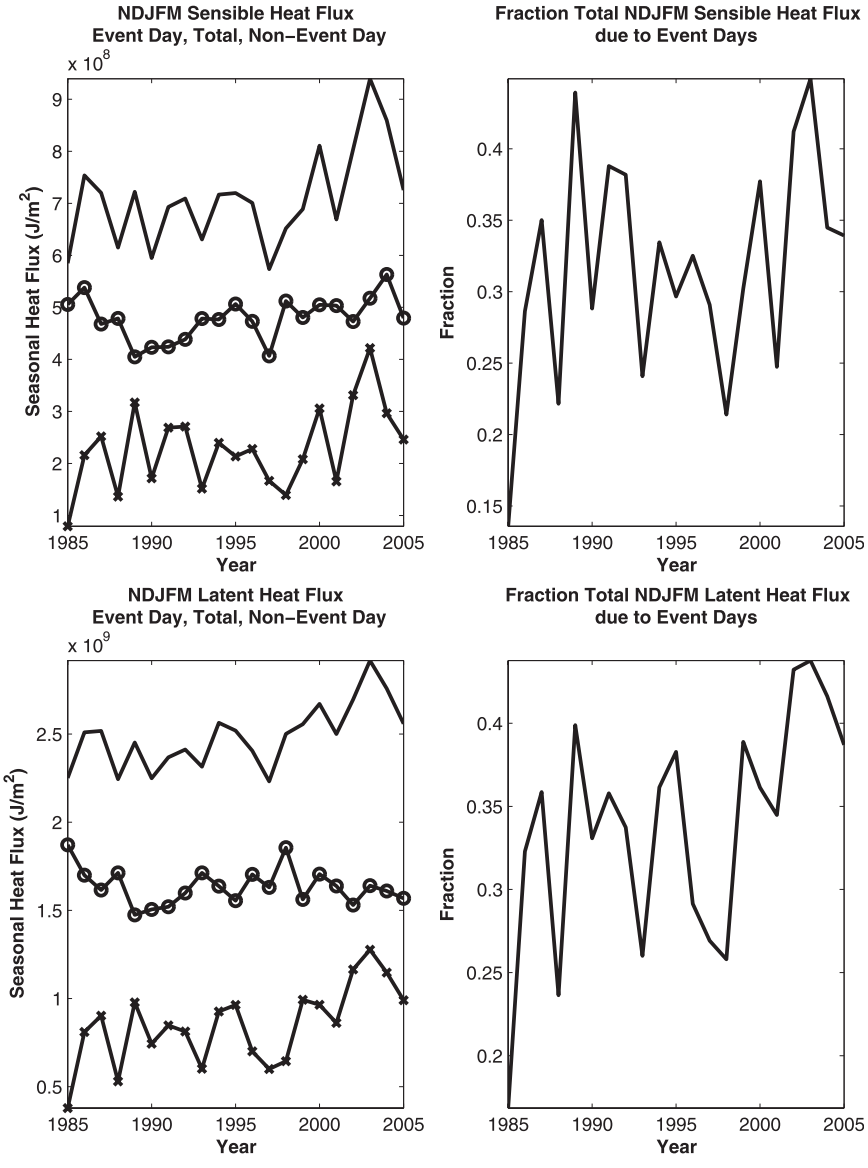

FIG. 7. As in Fig. 6, but for 1985–2005 NDFJM OAFlux project heat fluxes.

period (Fig. 6), so some caution is required in interpreting these results. However, similar trends are also evident for 1985–2005 in the shorter OAFlux record (Fig. 7). For their period of overlap, the NCEP–NCAR reanalysis and OAFlux time series of heat fluxes (Figs. 6 and 7) are highly correlated ($0.72 < r < 0.99$). None of these times series were correlated with the NDJFM NAO index at statistically significant levels (Table 2), which indicates that the seasonal variability of these turbulent fluxes is not linked to the NAO.

The distribution of the heat flux trends in and around the CLIMODE region can be seen in Fig. 8. Sensible and latent heat fluxes have increased with time off the eastern seaboard of North America. Previous work has identified a significant negative trend in 1948–2002 NCEP–NCAR reanalysis combined January–March (JFM) sensible and latent heat fluxes over waters centered around 35°N, 48°W (Gulev et al. 2007b). This location lies to the southeast of the positive trend shown in Figs. 8a,b. A negative trend is evident for this region in our analysis, too; however, it fails to reach statistical significance at $p < 0.10$ and is therefore not shown in Figs. 8a,b. The longer season examined (NDJFM) and longer record length (1949–2007) may explain this difference.

Over the last 60 years NDJFM surface and above-ground air temperatures have decreased over the northeastern United States, eastern Canada, and the Labrador Sea, while to the south over the ocean and CLIMODE

TABLE 1. Linear trends of summed 1948–2006 NCEP–NCAR reanalysis seasonal NDJFM CLIMODE region total, event, and nonevent day sensible and latent heat fluxes (J m^{-2} $decade^{-1}$). The trends for the fraction of total NDJFM heat flux occurring on event days, the number of event days per NDJFM season, and the average intensity of event day heat fluxes are also shown. Trends significant at $p < 0.05$ are in bold. The asterisk indicates significance at $p < 0.01$ and the double asterisk at $p < 0.005$. Correlations with time are presented in parentheses.

	Sensible heat flux	Latent heat flux
Total heat flux trend (J m^{-2} $decade^{-1}$)	**1.53×10^7**	**2.46×10^7**
	(0.32)	**(0.28)**
Event day trend (J m^{-2} $decade^{-1}$)	**1.64×10^7***	**4.24×10^7****
	(0.33)	**(0.37)**
Non-event day trend (J m^{-2} $decade^{-1}$)	-1.10×10^6	**-1.78×10^7**
	(−0.04)	**(−0.31)**
Trend of fraction of total heat flux	**0.013**	**0.014****
due to event days (proportion $decade^{-1}$)	**(0.29)**	**(0.37)**
Number of event days (days $decade^{-1}$)	**1.31***	**1.52****
	(0.34)	**(0.37)**
Average seasonal intensity of event day	0.40	0.52
heat fluxes (W m^{-2} $decade^{-1}$)	(0.08)	(0.08)

region they have increased (Figs. 8c–f). These opposing trends favor the observed seasonal increase of sensible and latent heat fluxes. That is, these trends indicate that at present *on average* colder surface air is advected off the continent and encounters warmer sea surface temperatures.

The cooling temperature trends north of roughly 40°N and the increases of CLIMODE region heat fluxes are due primarily to an increasing number of event days per NDJFM season—not an increasing intensity of heat fluxes during individual storm events (Table 1). This trend is indicative of changes in the frequency with which cold arctic air is exchanged with lower latitude air masses. Such changes are seen in the trend of upper tropospheric meridional wind variance (Fig. 9). During boreal winter, cold air masses develop over Canada and deepen from the surface upward. More frequent wintertime southward excursions of these cold air masses, indicated by the increasing trend of upper-level wind variance (Fig. 9), are consistent with an increased frequency of cold air outbreaks, as well as the decreasing surface and 2-m temperature trend over the northeastern United States and eastern Canada (Figs. 8c–f).

In essence, for the larger region, lower tropospheric flow has shifted to a more northerly course because of more frequent NDJFM synoptic storm activity over the last 60 years. At the same time, the Gulf Stream has advected increasingly warm subtropical waters poleward. These two trends have increased the surface and lower tropospheric temperature gradients in the vicinity of the Gulf Stream extension (Figs. 8c–f). In fact, the zero contour of the temperature shift runs parallel to and slightly north of the Gulf Stream extension. Over the last 60 years, the surface temperature difference spanning the 10° of latitude across this contour has increased by over 1 K (Fig. 8c).

We also examined monthly voluntary observing ship data within the CLIMODE region for consistency with the results obtained from the reanalysis. As described in the appendix, there is disagreement between the total NDJFM flux trends presented here (Figs. 6 and 7) and those derived from the monthly VOS data. The source of this discrepancy is uncertain, but as increasing event day heat fluxes associated with strong synoptic disturbances are the basis of the increasing total heat flux trend, it is possible and perhaps likely that the discrepancy between monthly VOS-derived estimates and those of the reanalysis and the OAFlux data stems from a fair-weather bias in which ships avoid the region during stormy weather (i.e., event days). These findings and issues are discussed at length in the appendix.

TABLE 2. Correlations of summed 1948–2006 NCEP–NCAR reanalysis seasonal NDJFM CLIMODE region total, event, and nonevent day sensible and latent heat fluxes with the NDJFM NAO index. No correlation coefficient (r) is statistically significant.

	NAO sensible heat flux	NAO latent heat flux
Total heat flux trend	−0.07	−0.14
Event day trend	0.02	−0.10
Non-event day trend	−0.17	−0.00
Trend of fraction of total heat flux due to event days	0.07	−0.09
Number of event days	0.00	−0.10
Average seasonal intensity of event day heat fluxes	0.08	−0.05

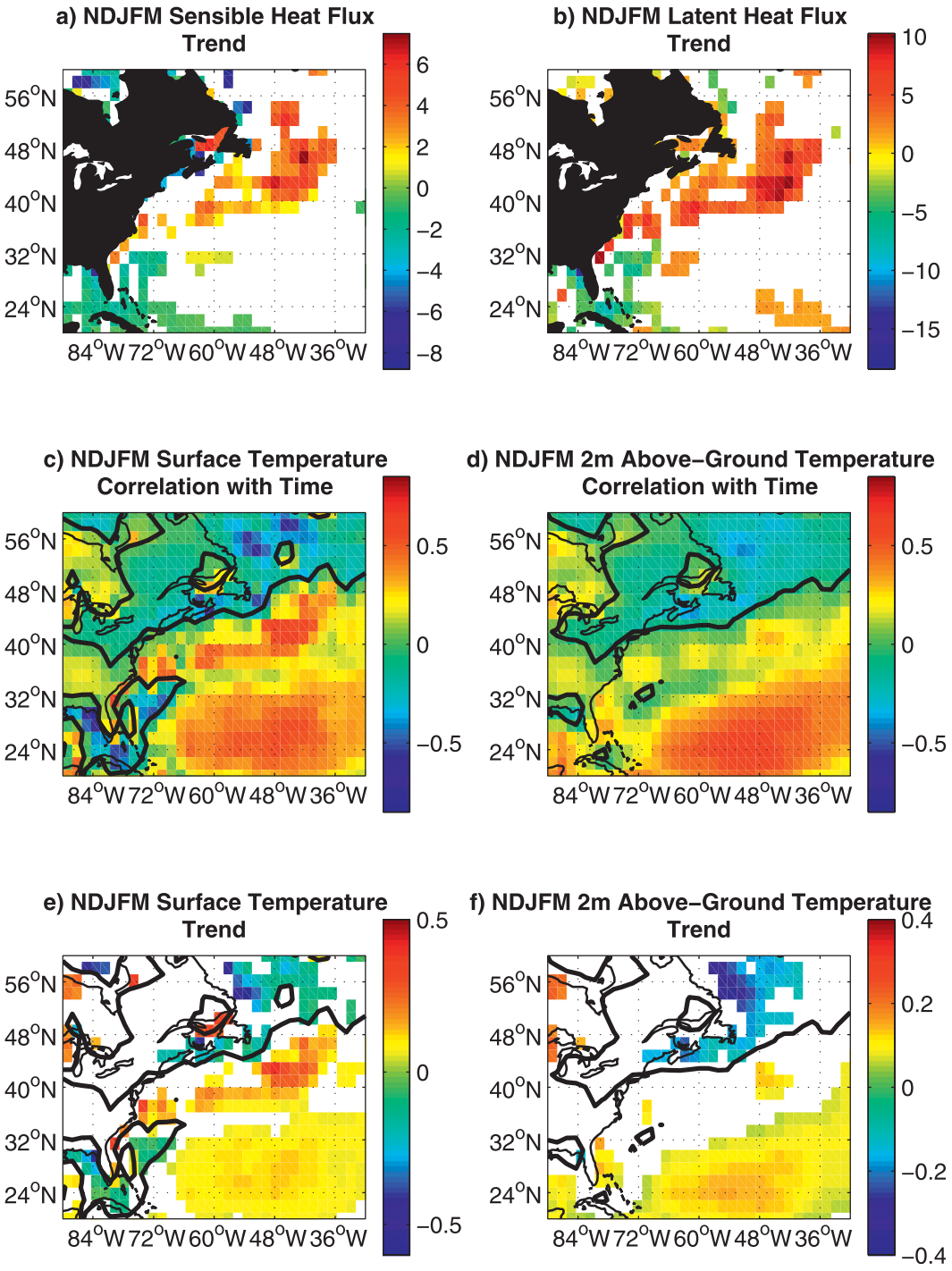

FIG. 8. Trends and correlations with time of 1949–2007 seasonal (NDJFM) NCEP–NCAR reanalysis fields. Trends (W m^{-2} $decade^{-1}$) for (a) sensible and (b) latent heat flux. Correlations with time of (c) surface temperature and (d) 2-m above ground temperature. Trends (K $decade^{-1}$) for (e) surface temperature and (f) 2-m above ground temperature. Calculations were made using monthly reanalysis. The thick black line is the zero correlation ($r = 0$) contour in (c) and (d) and the zero slope contour in (e) and (f). Only trends significant at the 90% level are shown.

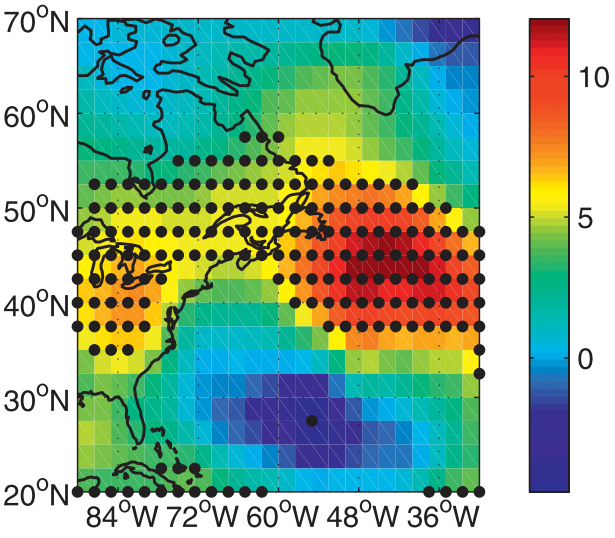

FIG. 9. Trend of 1948–2007 NDJFM NCEP–NCAR reanalysis daily meridional wind variance. Units are $m^2\ s^{-2}$ $decade^{-1}$. The field was calculated using daily reanalysis. Regions significant at the 95% level ($p < 0.05$) are dotted with black circles.

Storm activity indicators

We next explore storm activity trends over the North Atlantic through more direct measures. Two diagnostics were used. The first, 850-hPa eddy heat flux ($\overline{v'T'}$), is used to identify atmospheric fluctuations associated with local storm activity. A Butterworth filter with a half-power cutoff period of 8 days was used to high-pass filter the reanalysis record and select for variability at synoptic time scales. Here $\overline{v'T'}$ is also proportional to the vertical component of the Eliassen–Palm (E–P) flux vector (Hoskins et al. 1983). Positive values (upward E–P flux) imply strong downward transport of mean flow momentum, which reduces vertical shear and baroclinicity. The second diagnostic is a measure of low-level baroclinicity—specifically, the near-surface Eady growth rate maximum (Lindzen and Farrell 1980; Hoskins and Valdes 1990):

$$\sigma_{\mathrm{BI}} = 0.31 f \left| \frac{\partial \mathbf{v}}{\partial z} \right| N^{-1},$$

where f is the Coriolis parameter, $\mathbf{v} = (u, v)$ is the horizontal wind velocity, and N is the Brunt–Väisälä frequency. This metric was evaluated at 700 hPa.

Figure 10 shows the 60-yr mean $\overline{v'T'}$ and σ_{BI} for the North Atlantic. A region of high eddy heat flux is centered at 45°N, 54°W and has a slight southwest to northeast orientation. The mean σ_{BI} has a similar orientation but is shifted to the west and south off Cape Hatteras with a maximum at 36°N and 72°W. The Eady growth rate maximum is a metric of cyclone intensification potential; extratropical storms that develop and intensify in response to regions of high σ_{BI} grow as they propagate downstream in midlatitude westerlies. Thus, it is expected that zones of maximum baroclinicity lie upstream from regions of maximum eddy heat flux. This offset is consistent with previous analyses (Hoskins and Valdes 1990; Paciorek et al. 2002).

Trends of increasing $\overline{v'T'}$ and σ_{BI} are observed across the North Atlantic north of 40°N (Fig. 11). At 700 hPa, the increase in eddy heat flux over the 60-yr reanalysis record extends from North America to the British Isles, though there is a minimum around 33°W. At 850 hPa, the region with a positive trend of eddy heat flux extends south of 40°N along the North American coast over the

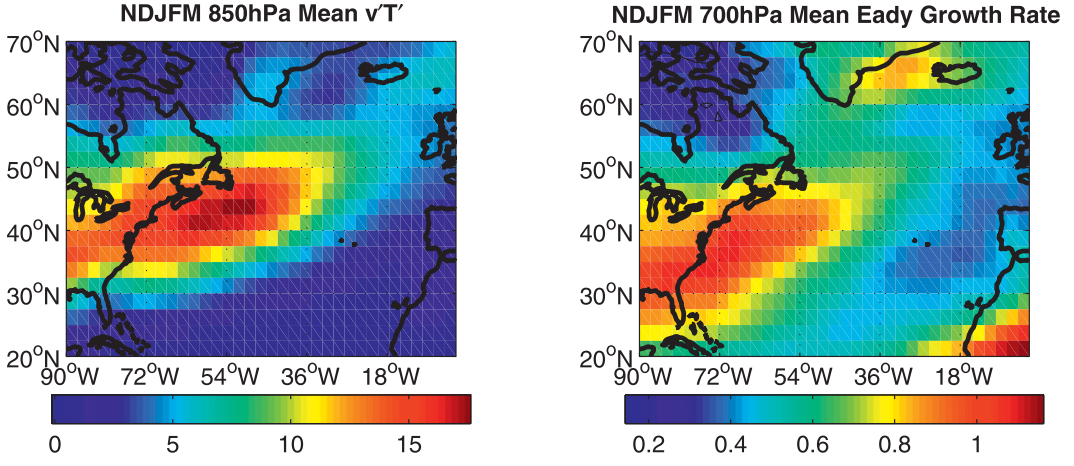

FIG. 10. 1948–2007 NDJFM NCEP–NCAR reanalysis climatologies of (left) 850 hPa 8-day high-pass filtered $\overline{v'T'}$ and (right) 700-hPa Eady growth rate maximum. Units are m K s^{-1} and day^{-1}. Fields were calculated using daily reanalysis.

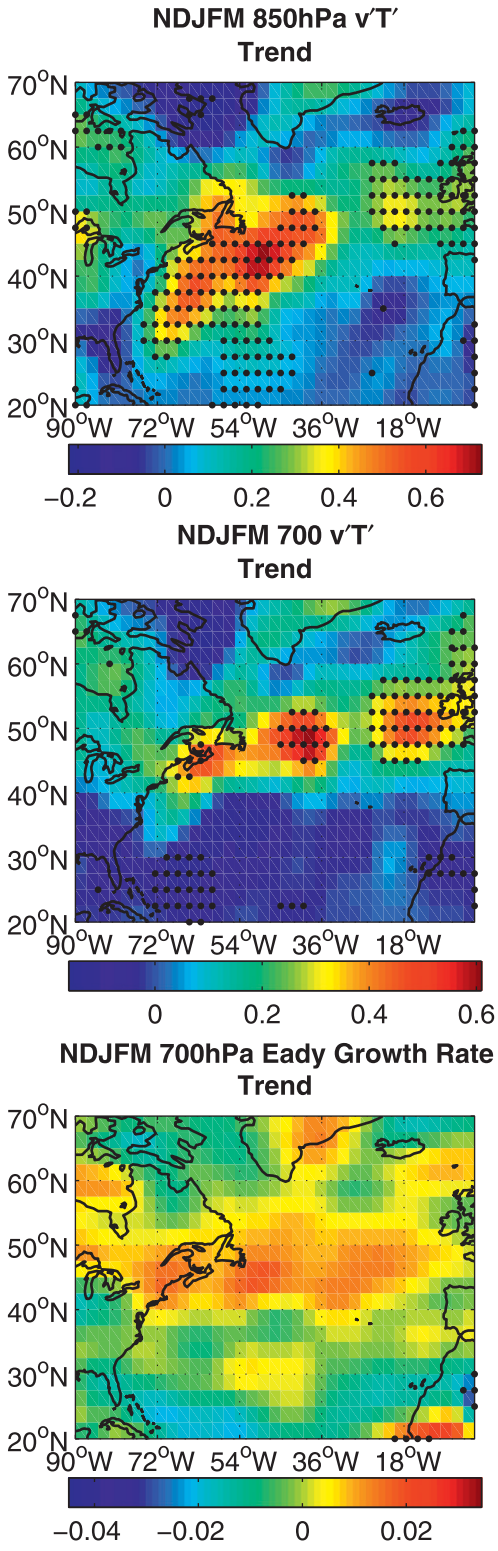

FIG. 11. 1948–2007 NDJFM NCEP–NCAR reanalysis seasonal trends of (top) 850-hPa 8-day high-pass filtered $\overline{v'T'}$ (m K s^{-1} decade^{-1}), (middle) 700-hPa 8-day high-pass filtered $\overline{v'T'}$ (m K s^{-1} decade^{-1}), and (bottom) 700-hPa Eady growth rate maximum (day^{-1} decade^{-1}). Fields were calculated using daily reanalysis. Regions significant at the 95% level ($p < 0.05$) are dotted with black circles.

western North Atlantic (Fig. 11a). These trends in storm activity are broadly consistent with previous findings for this region, which show increasing wintertime storm activity between 40° and 50°N over the North Atlantic (Geng and Sugi 2001; Gulev et al. 2001; 2002; Chang and Fu 2002; Paciorek et al. 2002; Harnik and Chang 2003; Chang 2007). The 700-hPa σ_{BI} trend pattern corresponds most closely to the 700-hPa $\overline{v'T'}$ and demonstrates an increase in mean wintertime low-level baroclinicity along the North Atlantic storm track (Fig. 11c).

The changes to 700-hPa σ_{BI} north of 40°N are principally the result of increasing low-level vertical wind shear along the storm track (Fig. 12). The pattern of increasing 700-hPa wind shear also matches the trend pattern for 700-hPa $\overline{v'T'}$. Changes to the Brunt–Väisälä frequency over the open ocean also increase the growth rate diagnostic north of 45°N, but appear to be of secondary importance; along the North American coast and near the British Isles north of 40°N where σ_{BI} increases, N also increases with time north of 40°N, which should instead reduce σ_{BI} in this region.

The 700-hPa wind shear trend reflects changes in the horizontal temperature gradient. Such temperature changes can be seen in the surface (T_s) and 2-m temperature (T_a) trend plots (Figs. 8c–f), which show an increasing temperature gradient just north of the Gulf Stream extension. These same temperature changes, which alter the horizontal temperature gradient and consequently low-level wind shear, baroclinicity, and storm activity, also produce the change in the near-surface vertical temperature gradient ($T_s - T_a$) that drives the trends in surface sensible and latent heat fluxes over the CLIMODE region. In fact, the trend of $T_s - T_a$ (Fig. 13) corresponds well with these turbulent flux trends (Figs. 8a,b), suggesting that the changes in the large-scale fields are also affecting the flux trends and not merely responding to them.

6. Discussion

Synoptic storm activity over the CLIMODE region during winter brings cold air from the north off the North American continent and over warm Gulf Stream waters. During these synoptic events surface sensible and latent heat fluxes are greatly elevated and mode water formation is enhanced. Owing to these storm events, around 41% (34%) of the 1948–2007 total NDJFM sensible (latent) heat flux occurs during just 17% (20%) of NDJFM days. Thus, much of the seasonal heat loss from CLIMODE region surface waters occurs episodically.

In addition, the number of storm event days and the proportion of total NDJFM sensible and latent ocean-to-atmosphere heat flux that occurs during event days

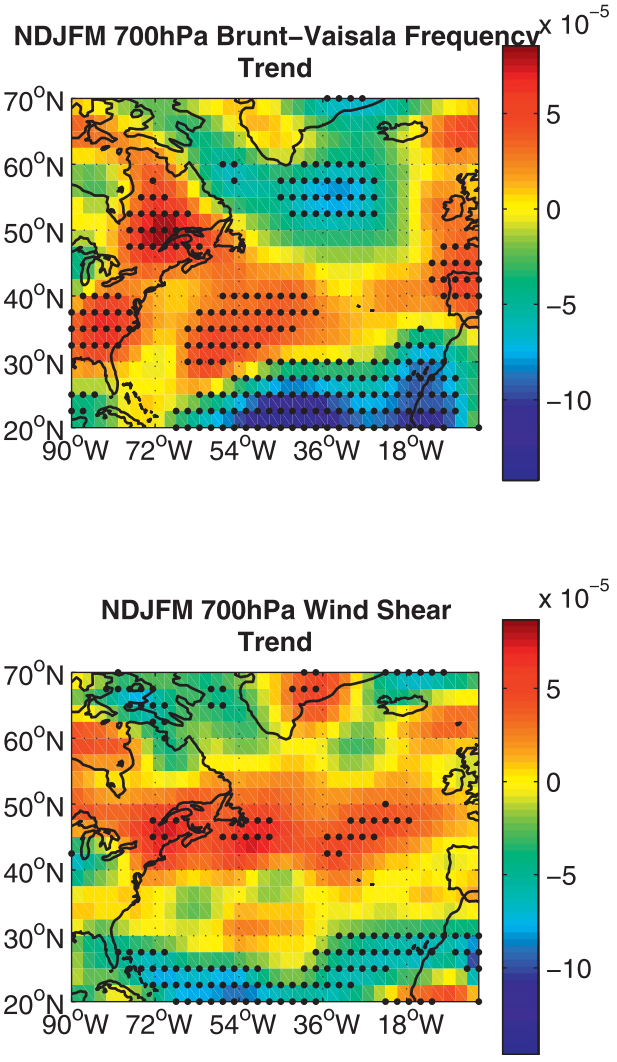

FIG. 12. 1948–2007 NDJFM NCEP–NCAR reanalysis trends of (top) 700-hPa Brunt–Väisälä frequency (s^{-1} decade^{-1}) and (bottom) 700-hPa wind shear (m s^{-1} decade^{-1}). Fields were calculated using daily reanalysis. Regions significant at the 95% level ($p < 0.05$) are dotted with black circles.

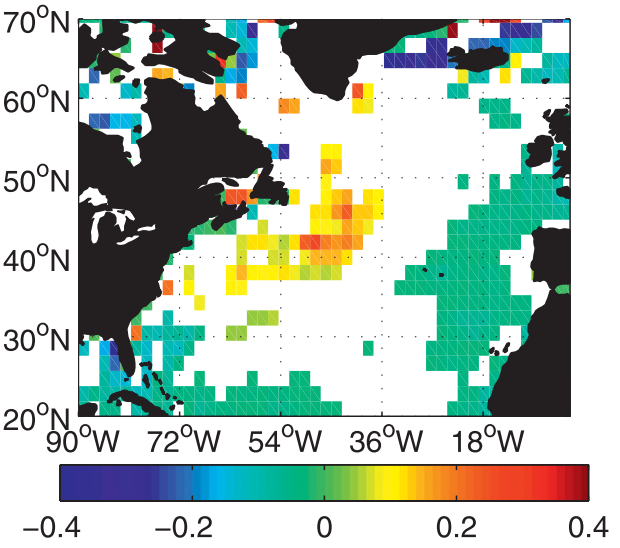

FIG. 13. 1949–2007 NDJFM NCEP–NCAR reanalysis trend of the difference between surface and 2-m temperature. Units are K decade^{-1}. The field was calculated using monthly reanalysis. Only trends significant at the 95% level ($p < 0.05$) are shown.

have increased over the last 60 years. This increased storm frequency (i.e., more cold air outbreaks) has produced changes to the mean state in the vicinity of the Gulf Stream Extension and STMW outcrop, including decreased surface and 2-m air temperature over the northeastern United States, eastern Canada, and the Labrador Sea, and has possibly contributed to the increased surface and 2-m air temperature to the south-southeast over the Sargasso Sea.

The cooling trend north of 40°N (Figs. 8c,d) appears to be the consequence of factors specific to the region. Consistent with quasigeostrophic theory, westerly flow over the Rocky Mountains produces a downstream north–south standing wave that directs mean northwesterly flow offshore and over the Gulf Stream (Figs. 3c,d). Thus, orography and the North Atlantic western boundary current create a strong baroclinic zone where cold wintertime Canadian air is advected over warm ocean waters. A recent modeling study shows that the combined effects of Rocky Mountain–like orography and land–sea temperature contrast synergistically concentrate synoptic activity around the latitude of the continental margin (Gerber and Vallis 2009). In response to greenhouse gas forcing, many climate models project increasing extratropical storm activity. Over North America, the increased storm activity will likely organize in this region of mean northwesterly flow and strong low-level temperature gradients. While the synoptic storms act to reduce the temperature gradient by transporting heat poleward, the increased mean northerly flow off the continent acts to cool the ocean surface north of 40°N. This effect, coupled with the warming ocean water temperatures south of 40°N, appears to have strengthened the low-level temperature gradient (Figs. 8c–f).

Through the thermal wind response, the increased low-level temperature gradient at 40°N has produced concomitant increases of low-level wind shear and baroclinicity along the North Atlantic storm track. The 700-hPa σ_{BI} trend is greatest north of the climatological maximum of low-level σ_{BI} off the Carolinas (Fig. 10) and indicates that the region of optimal storm intensification may be shifting northward. The wind shear and σ_{BI} changes are accompanied by increased storm activity across the North Atlantic north of 40°N and may, in fact, favor this increased storm activity. Thus, these trends

suggest a positive feedback in which the increased storm activity, through intensification of the horizontal temperature gradient along the Gulf Stream at the upstream end of the storm track, creates conditions favorable for more cyclogenesis in this region.

Increased diabatic heating of the lower troposphere due to increased surface heat fluxes can itself fuel synoptic storm events (Mak 1998); however, a decreasing trend of N over the CLIMODE region is not observed. Thus, the increased surface heat fluxes over the CLIMODE region appear to be a response to the changes in storm activity and do not themselves appear to feed back positively on the trend of increasing storm activity.

The trends described here, particularly for the surface turbulent fluxes, may be corrupted by changes in the assimilation of observations or upgrades to the NCEP–NCAR reanalysis model (Yuan et al. 2009), changes in the frequency of shipboard and mooring measurements (Gulev et al. 2007b), changes to measurement methods (Kent et al. 2007), or observational errors (Chang 2007). However, the legitimacy of the surface flux trends described here is supported by the concurrent trends of other large-scale atmospheric fields captured by the reanalysis model and constrained by more voluminous terrestrial surface, radiosonde, dropsonde, and satellite observations. Ongoing evaluation of these trends in the coming years and further study of the proposed feedback mechanism are needed to validate these findings.

Previous studies have shown that the NAO is associated with storm activity over the North Atlantic and may, in fact, be a manifestation of this storm track (Vallis and Gerber 2008; Gerber and Vallis 2009). Our results here, however, indicate that CLIMODE region turbulent fluxes, including those associated with cold air outbreaks, are independent of the NAO at seasonal and longer time scales. This circumstance may result from geography, as the CLIMODE region resides at the westernmost portion of the North Atlantic storm track.

The overall increase of NDJFM sensible and latent heat fluxes in the CLIMODE region over the last 60 years indicates that the synoptic-scale atmospheric processes facilitating seasonal North Atlantic mode water formation have themselves changed. Long-term changes in STMW properties may occur on multidecadal time scales, and it has been argued that such changes may reflect shifts in storm track position, which alter regions of high air–sea fluxes, freshwater input, and oceanic convection (Dickson et al. 1996). The changes to eddy heat flux and low-level baroclinicity in the North Atlantic (Fig. 11) may indicate that such a shift has been and is occurring.

Acknowledgments. We thank Nicholas Bond, Jimmy Booth, Steve Esbensen, Justin Small, and Robert Weller for helpful discussions. This work was funded by NSF Grant OCE-0424516.

APPENDIX

We additionally looked for trends in CLIMODE region monthly estimates of sensible and latent heat fluxes based on voluntary observing ship data. Specifically, we used 1948–93 flux estimates derived from the Comprehensive Ocean–Atmosphere Dataset (COADS) (Da Silva et al. 1994) and the 1973–2005 National Oceanography Center, Southampton (NOCS) Surface Flux Dataset version 2.0 (Berry and Kent 2009), which optimally interpolates the International COADS (ICOADS) release 2.4 ship data. These data are monthly and can only be used for assessment of total seasonal NDJFM turbulent flux trends; that is, no event day trend analyses can be performed.

Only the NOCS NDJFM latent heat fluxes displayed a statistically significant increasing trend (Fig. A1). NOCS NDJFM sensible heat fluxes and the COADS-derived (Da Silva et al. 1994) NDJFM sensible and latent heat fluxes show no trend. These results are at odds with the total NDJFM trend findings of NCEP–NCAR reanalysis and OAFlux data (Figs. 6 and 7). The NOCS dataset does provide a number of error estimates. For the CLIMODE region, there are significant positive trends in the random and total error of the flux estimates for this region (Fig. A1). For the sensible heat fluxes, the magnitudes of some of these error trends are larger than the nonsignificant sensible heat flux trend.

Correlations of total seasonal (NDJFM) sensible and latent heat fluxes averaged for the CLIMODE region are shown in Tables A1 and A2. For the NDJFM season, the interannual variability of the NCEP–NCAR reanalysis and OAFlux estimates are most closely matched. The NOCS estimates are also well correlated ($r = 0.88$–0.93) with the NCEP–NCAR reanalysis and OAFlux estimates; however, the COADS-derived estimates are less well matched ($r = 0.67$–0.73).

Gulev et al. (2007a,b) have shown there are considerable biases in ICOADS observations and that linear trends of turbulent fluxes can vary considerably between reanalysis- and ICOADS-derived data. Over the CLIMODE region these include random sampling uncertainties, interpolation uncertainties, and fair-weather bias. These appear to lead to biases of 10–20 W m^{-2} over the Gulf Stream extension and SMTW outcrop region (Gulev et al. 2007a). Whether changes in these biases through time for the CLIMODE region would lead to spurious trend features (or the absence of a trend, in this instance) is difficult to ascertain; however, Gulev et al. (2007b) found patches of significant differences between

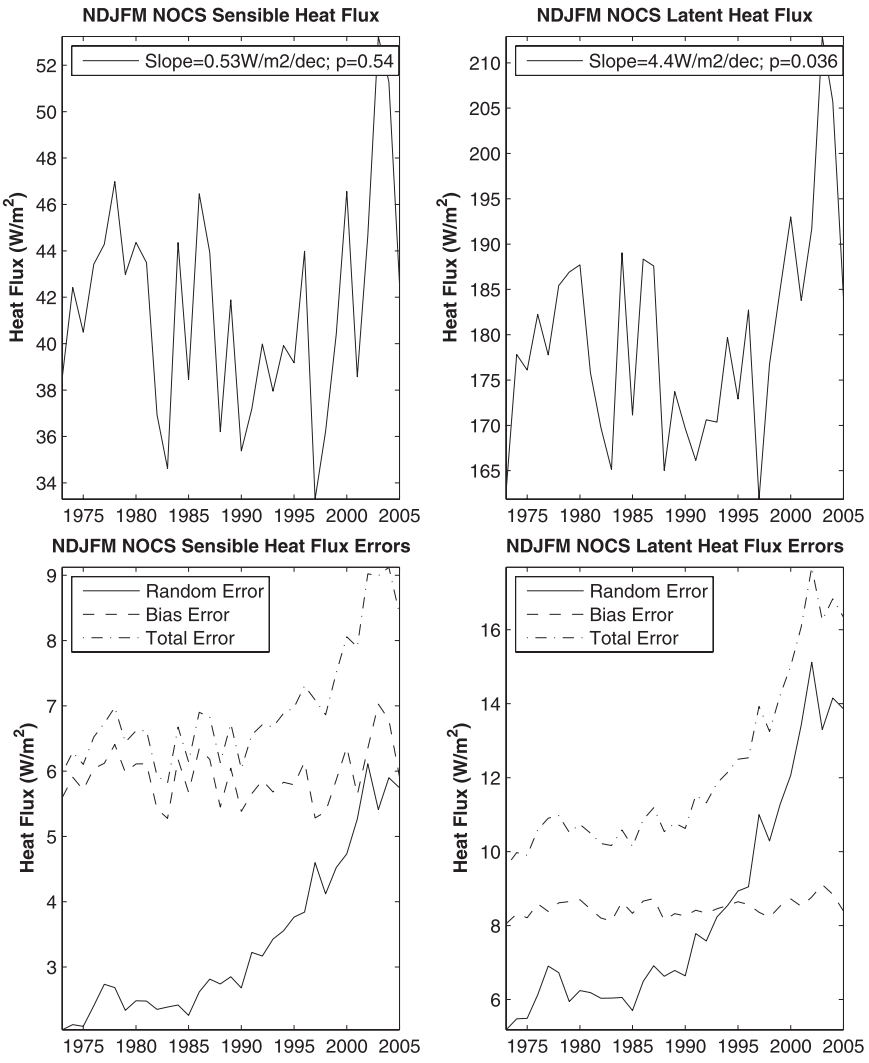

FIG. A1. Time series of the NOCS surface flux dataset version 2.0 heat flux data. (top left) 1973–2005 NDJFM sensible heat flux time series; (top right) 1973–2005 NDJFM latent heat flux time series; (bottom left) sensible heat flux error time series; (bottom right) latent heat flux error time series. Linear trend slope estimates are shown in the legend of each panel.

the linear trends of JFM NCEP–NCAR reanalysis and ICOADS within our study region. Chang (2007) also found large observational errors of shipboard pressure within the ICOADS record during the late 1960s and early 1970s. These errors were found to reduce the increasing storm activity trend over the Atlantic.

For this study, the fair-weather bias is of particular concern. This work focuses on high flux (storm) events, and these are the very events that ships avoid. If ships avoid the CLIMODE region during bad weather, VOS-based estimates of turbulent fluxes will underestimate or miss entirely the storm contribution to the overall trend. Indeed, it is the increasing frequency of high flux (storm) events that forms the basis of the increasing trend of total NDJFM sensible and latent heat fluxes within the NCEP–NCAR reanalysis and OAFlux records (Figs. 6 and 7). For datasets based primarily on shipboard measurements, such as the NOCS- and COADS-derived, the potential sampling bias against high flux event datasets

TABLE A1. Correlations of NDJFM seasonal sensible heat fluxes for the CLIMODE region. Comparison is between 1948–2006 NCEP–NCAR reanalysis, 1985–2005 OAFlux estimates, 1948–93 COADS-derived (Da Silva et al. 1994) flux estimates, and 1973–2005 NOCS (ICOADS) flux estimates.

	NCEP	OAFlux	Da Silva	NOCS
NCEP	1.00	0.99	0.73	0.88
OAFlux	0.99	1.00	0.72	0.93
Da Silva	0.73	0.72	1.00	0.95
NOCS	0.88	0.93	0.95	1.00

TABLE A2. Correlations of NDJFM seasonal latent heat fluxes for the CLIMODE region. Comparison is between 1948–2006 NCEP–NCAR reanalysis, 1985–2005 OAFlux estimates, 1948–93 COADS-derived (Da Silva et al. 1994) flux estimates, and 1973–2005 NOCS (ICOADS) flux estimates.

	NCEP	OAFlux	Da Silva	NOCS
NCEP	1.00	0.98	0.67	0.92
OAFlux	0.98	1.00	0.68	0.92
Da Silva	0.67	0.68	1.00	0.92
NOCS	0.92	0.92	0.92	1.00

within the CLIMODE region is large given that, coming off the continent as they do, many of these storms are well forecast.

Indeed, we examined the raw 6-hourly ICOADS data for differences in the number of observations per day within the CLIMODE region during NDJFM event and nonevent days. Based on a simple two-way analysis of variance (ANOVA) test we found significantly fewer observations per event day than per nonevent day ($p = 0.013$). This finding supports the notion that a fair-weather bias exists within the CLIMODE region.

In addition to the likelihood of a fair-weather bias, which leads us to discount the results of the COADS and NOCS trend analyses, a complementary factor that supports the reality of the turbulent flux trends depicted by NCEP–NCAR reanalysis and OAFlux estimates (Figs. 6 and 7) is the concomitant trends of other large-scale atmospheric fields captured by the reanalysis model and constrained by more voluminous terrestrial surface, radiosonde, dropsonde, and satellite observations. For the CLIMODE region, these include land surface temperatures, upper-level wind variance, and lower tropospheric eddy heat fluxes and Eady growth rates. The tendencies of these trends are consistent with increasing heat flux trends. Gulev et al. (2007b) also suggest that reanalysis provides a better platform for studying climatological trends, as these estimates are better constrained by the various assimilated terrestrial and atmospheric observations, and the models used to make these estimates have demonstrated skill making medium-range forecasts.

REFERENCES

Alexander, M. A., and C. Deser, 1995: A mechanism for the recurrence of wintertime midlatitude SST anomalies. *J. Phys. Oceanogr.,* **25,** 122–137.

——, and J. D. Scott, 1997: Surface flux variability over the North Pacific and North Atlantic Oceans. *J. Climate,* **10,** 2963–2978.

Bane, J. M., and K. E. Osgood, 1989: Wintertime air–sea interaction processes across the Gulf Stream. *J. Geophys. Res.,* **94,** 10 755–10 772.

Benedict, J. J., S. Lee, and S. B. Feldstein, 2004: Synoptic view of the North Atlantic Oscillation. *J. Atmos. Sci.,* **61,** 121–144.

Berry, D. I., and E. C. Kent, 2009: A new air–sea interaction gridded dataset from ICOADS with uncertainty estimates. *Bull. Amer. Meteor. Soc.,* **90,** 645–656.

Bond, N. A., and M. F. Cronin, 2008: Regional weather patterns during anomalous air–sea fluxes at the Kuroshio Extension Observatory (KEO). *J. Climate,* **21,** 1680–1697.

Brayshaw, D. J., B. Hoskins, and M. Blackburn, 2008: The storm-track response to idealized SST perturbations in an aqua-planet GCM. *J. Atmos. Sci.,* **65,** 2842–2860.

Cayan, D. R., 1992: Latent and sensible heat-flux anomalies over the northern oceans: The connection to monthly atmospheric circulation. *J. Climate,* **5,** 354–369.

Chang, E. K. M., 2007: Assessing the increasing trend in Northern Hemisphere winter storm track activity using surface ship observations and a statistical storm track model. *J. Climate,* **20,** 5607–5628.

——, and Y. Fu, 2002: Interdecadal variations in Northern Hemisphere winter storm track intensity. *J. Climate,* **15,** 642–658.

Colucci, S. J., 1976: Winter cyclone frequencies over the eastern United States and adjacent western Atlantic 1964–1973. *Bull. Amer. Meteor. Soc.,* **57,** 548–553.

da Silva, A. M., C. C. Young, and S. Levitus, 1994: *Anomalies of Heat and Momentum Fluxes.* Vol. 3, *Atlas of Surface Marine Data 1994,* NOAA Atlas NESDIS 8, 413 pp.

Deser, C., and M. S. Timlin, 1997: Atmosphere–ocean interaction on weekly timescales in the North Atlantic and Pacific. *J. Climate,* **10,** 393–408.

Dewar, W. K., R. M. Samelson, and G. K. Vallis, 2005: The ventilated pool: A model of subtropical mode water. *J. Phys. Oceanogr.,* **35,** 137–150.

Dickson, R., J. Lazier, J. Meincke, P. Rhines, and J. Swift, 1996: Long-term coordinated changes in the convective activity of the North Atlantic. *Prog. Oceanogr.,* **38,** 241–295.

Esbensen, S. K., and Y. Kushnir, 1981: Heat budget of the global ocean: Estimates from surface marine observations. Climate Research Institute Rep. 29, Oregon State University, Corvallis, OR, 271 pp.

Fairall, C. W., E. F. Bradley, J. E. Hare, A. A. Grachev, and J. B. Edson, 2003: Bulk parameterization of air–sea fluxes: Updates and verification for the COARE algorithm. *J. Climate,* **16,** 571–591.

Geng, Q., and M. Sugi, 2001: Variability of the North Atlantic cyclone activity in winter analyzed from NCEP–NCAR reanalysis data. *J. Climate,* **14,** 3863–3873.

Gerber, E. P., and G. K. Vallis, 2009: On the zonal structure of the North Atlantic Oscillation and annular modes. *J. Atmos. Sci.,* **66,** 332–352.

Gulev, S. K., O. Zolina, and S. Grigoriev, 2001: Extratropical cyclone variability in the Northern Hemisphere winter from the NCEP/NCAR reanalysis data. *Climate Dyn.,* **17,** 795–809.

——, T. Jung, and E. Ruprecht, 2002: Climatology and interannual variability in the intensity of synoptic-scale processes in the North Atlantic from the NCEP–NCAR reanalysis data. *J. Climate,* **15,** 809–828.

——, ——, and ——, 2007a: Estimation of the impact of sampling errors in the VOS observations on air–sea fluxes. Part I: Uncertainties in climate means. *J. Climate,* **20,** 279–301.

——, ——, and ——, 2007b: Estimation of the impact of sampling errors in the VOS observations on air–sea fluxes. Part II: Impact on trends and interannual variability. *J. Climate,* **20,** 303–315.

Harnik, N., and E. K. M. Chang, 2003: Storm track variations as seen in radiosonde observations and reanalysis data. *J. Climate,* **16,** 480–495.

Hoskins, B. J., and P. J. Valdes, 1990: On the existence of storm tracks. *J. Atmos. Sci.,* **47,** 1854–1864.

——, I. N. James, and G. H. White, 1983: The shape, propagation, and mean-flow interaction of large-scale weather systems. *J. Atmos. Sci.,* **40,** 1595–1612.

——, M. E. McIntyre, and A. W. Robertson, 1985: On the use and significance of isentropic potential vorticity maps. *Quart. J. Roy. Meteor. Soc.,* **111,** 877–947.

Inatsu, M., H. Mukougawa, and S.-P. Xie, 2003: Atmospheric response to zonal variations in midlatitude SST: Transient and stationary eddies and their feedback. *J. Climate,* **16,** 3314–3329.

Jin, F.-F., L.-L. Pan, and M. Watanabe, 2006: Dynamics of synoptic eddy and low-frequency flow interaction. Part II: A theory for low-frequency modes. *J. Atmos. Sci.,* **63,** 1695–1708.

Josey, S. A., E. C. Kent, and P. K. Taylor, 1999: New insights into the ocean heat budget closure problem from analysis of the SOC air–sea flux climatology. *J. Climate,* **12,** 2856–2880.

Joyce, T. M., C. Deser, and M. A. Spall, 2000: The relation between decadal variability of subtropical mode water and the North Atlantic oscillation. *J. Climate,* **13,** 2550–2569.

Kalnay, E., and Coauthors, 1996: NCEP/NCAR 40-Year Reanalysis Project. *Bull. Amer. Meteor. Soc.,* **77,** 437–471.

Kelly, K. A., R. J. Small, R. M. Samelson, B. Qiu, T. Joyce, Y.-O. Kwon, and M. Cronin, 2010: Western boundary currents and frontal air–sea interaction: Gulf Stream and Kuroshio Extension. *J. Climate,* in press.

Kent, E. C., S. D. Woodruff, and D. I. Berry, 2007: Metadata from WMO Publication No. 47 and an assessment of voluntary observing ship observation heights in ICOADS. *J. Atmos. Oceanic Technol.,* **24,** 214–234.

Lindzen, R. S., and B. Farrell, 1980: A simple approximate result for the maximum growth rate of baroclinic instabilities. *J. Atmos. Sci.,* **37,** 1648–1654.

Mak, M., 1998: Influence of surface sensible heat flux on incipient marine cyclogenesis. *J. Atmos. Sci.,* **55,** 820–834.

Marshall, J., and Coauthors, 2009: The CLIMODE field campaign: Observing the cycle of convection and restratification over the Gulf Stream. *Bull. Amer. Meteor. Soc.,* **90,** 1337–1350.

Nakamura, H., T. Sampe, Y. Tanimoto, and A. Shimpo, 2004: Observed associations among storm tracks, jet streams and midlatitude oceanic fronts. *Earth's Climate: The Ocean–Atmosphere Interaction, Geophys. Monogr.,* Vol. 147, Amer. Geophys. Union, 329–345.

——, ——, A. Goto, W. Ohfuchi, and S.-P. Xie, 2008: On the importance of midlatitude oceanic frontal zones for the mean state and dominant variability in the tropospheric circulation. *Geophys. Res. Lett.,* **35,** L15709, doi:10.1029/2008GL034010.

Paciorek, C. J., J. S. Risbey, V. Ventura, and R. D. Rosen, 2002: Multiple indices of Northern Hemisphere cyclone activity, winters 1949–99. *J. Climate,* **15,** 1573–1590.

Patoux, J., X. Yuan, and C. Li, 2009: Satellite-based midlatitude cyclone statistics over the Southern Ocean: 1. Scatterometer-derived pressure fields and storm tracking. *J. Geophys. Res.,* **114,** D04105, doi:10.1029/2008JD010873.

Sanders, F., 1986: Explosive cyclogenesis in the west-central North Atlantic Ocean, 1981–84. Part I: Composite structure and mean behavior. *Mon. Wea. Rev.,* **114,** 1791–1794.

——, and J. R. Gyakum, 1980: Synoptic-dynamic climatology of the ''bomb.'' *Mon. Wea. Rev.,* **108,** 1589–1606.

Talley, L. D., 1996: North Atlantic circulation and variability, reviewed for the CNLS conference. *Physica D,* **98,** 625–646.

Vallis, G. K., and E. P. Gerber, 2008: Local and hemispheric dynamics of the North Atlantic Oscillation, annular patterns and the zonal index. *Dyn. Atmos. Oceans,* **44,** 184–212.

Worthington, L. V., 1959: The 18°C Water in the Sargasso Sea. *Deep-Sea Res.,* **5,** 297–305.

Yu, L., X. Jin, and R. A. Weller, 2008: Multidecade global flux datasets from the Objectively Analyzed Air–Sea Fluxes (OAFlux) project: Latent and sensible heat fluxes, ocean evaporation, and related surface meteorological variables. OAFlux Project Tech. Rep. OA-2008-01, Woods Hole Oceanographic Institution, 64 pp.

Yuan, X., J. Patoux, and C. Li, 2009: Satellite-based midlatitude cyclone statistics over the Southern Ocean: 2. Tracks and surface fluxes. *J. Geophys. Res.,* **114,** D04106, doi:10.1029/2008JD010874.

Zolina, O., and S. K. Gulev, 2003: Synoptic variability of ocean–atmosphere turbulent fluxes associated with atmospheric cyclones. *J. Climate,* **16,** 2717–2734.